Short- and long-range topological correlations in two-dimensional aggregation of dense colloidal suspensions

J. C. Fernández-Toledano,[1] A. Moncho-Jordá,[1] F. Martínez-López,[1] A. E. González,[2] and R. Hidalgo-Álvarez[1]
[1]*Departamento de Física Aplicada, Facultad de Ciencias, Campus Fuentenueva S/N, 18071 Granada, Spain*
[2]*Centro de Ciencias Físicas, Universidad Nacional Autónoma de México, Apartado Postal 48-3, 62251 Cuernavaca, Morelos, México*
(Received 11 November 2004; revised manuscript received 28 January 2005; published 7 April 2005)

We have studied the average properties and the topological correlations of computer-simulated two-dimensional (2D) aggregating systems at different initial surface packing fractions. For this purpose, the centers of mass of the growing clusters have been used to build the Voronoi diagram, where each cell represents a single cluster. The number of sides (n) and the area (A) of the cells are related to the size of the clusters and the number of nearest neighbors, respectively. We have focused our paper in the study of the topological quantities derived from number of sides, n, and we leave for a future work the study of the dependence of these magnitudes on the area of the cells, A. In this work, we go beyond the adjacent cluster correlations and explore the organization of the whole system of clusters by dividing the space in concentric layers around each cluster: the shell structure. This method allows us to analyze the time behavior of the long-range intercluster correlations induced by the aggregation process. We observed that kinetic and topological properties are intimately connected. Particularly, we found a continuous ordering of the shell structure from the earlier stages of the aggregation process, where clusters positions approach a hexagonal distribution in the plane. For long aggregation times, when the dynamic scaling regime is achieved, the short- and long-range topological properties reached a final stationary state. This ordering is stronger for high particle densities. Comparison between simulation and theoretical data points out the fact that 2D colloidal aggregation in the absence of interactions (diffusion-limited cluster aggregation regimen) is only able to produce short-range cluster-cluster correlations. Moreover, we showed that the correlation between adjacent clusters verifies the Aboav-Weaire law, while all the topological properties for nonadjacent clusters are mainly determined by only two parameters: the second central moment of number-of-sides distribution $\mu_2=\Sigma P(n)(n-6)^2$ and the screening factor a (defined through the Aboav-Weaire equation). We also found that the values of μ_2 and a calculated for two-dimensional aggregating system are related through a single universal common form $a \propto \mu_2^{-0.89}$, which is independent of the particle concentration.

DOI: 10.1103/PhysRevE.71.041401 PACS number(s): 82.70.Dd, 02.50.−r

I. INTRODUCTION

The formation of colloidal monolayers is especially interesting due to the ability of colloidal particles to influence the stability of emulsions, foams, and interfacial properties. Particularly, the study of aggregation in colloidal systems confined in two dimensions has drawn wide attention due to the interesting observed effects, such as fractal cluster growth [1–3] or mesostructure formation [4,5]. At this respect, the structure of the clusters and the kinetic properties of the coagulation process have been investigated by means of both experiments and simulations [1–3,6]. Theoretically, the success of technics for treating phase transition phenomena has motivated the application of these ideas to the analysis of the scaling properties of the cluster-size distribution in aggregating systems [7,8]. The results show that the morphology of colloidal clusters is fractal scale invariant, and it is related to the time evolution of the cluster-size distribution.

Some years ago, other interesting aspects of colloidal coagulation have been applied to the study of dense colloidal suspension in two and three dimensions: intercluster spatial [9–14] and topological ordering [15–17]. These recent pictures complement the ones given by the kinetics and fractal growth description, and provide information about the organization of the colloidal clusters in the space. One of the most significant findings is the appearance of a maximum in the structure factor $S(q)$ at finite q for long aggregation times, which corresponds to a characteristic length scale of the system connected with the typical cluster-cluster separation. Moreover, the structure factor obtained at different times in the scaling regime can be expressed into a single time-independent common form. Also the topological properties have been found to reach a final stationary values. All these facts imply that the aggregation process induce structuring not only inside the fractal clusters, but also in the intercluster correlations, and indicate the necessity of being included in order to have a complete self-consistent theory of the aggregation phenomenon.

A very useful tool to determine the correlations and ordering in space-filling systems is the one based on the topological properties. Topology is the mathematical study of the properties that are preserved through deformation, twistings, and stretchings of objects. The study of the topological properties of such systems can be achieved with the help of the Voronoi construction, which creates a division of the whole space in irregular partitions (cells). Such a method has been successfully used to describe the evolution of many natural systems, such as soap froths [18–22], propagation of defects in foams [23,24], metallurgical grains [25], biological tissues [26], crack patterns in ceramics [27], etc. Even though these

systems differ in the way they evolve (mitosis for biological tissues, diffusion of gas between neighbor cells for soap froths, etc.), it is found that most of them arrive at a final stationary state where topological properties remain constant. Moreover, this state is described by the same common laws, which come from maximum entropy predictions [28,29]. However, all these works are essentially mean-field studies and only account for correlations between adjacent cells. In recent times, the description of the long-range topological ordering and the correlation between non-nearest neighbors have attracted interest and new theoretical methods based on shell structure have been applied to the understanding of the evolution of cellular systems [30–35].

In this work we focus our study on the topological properties of two-dimensional aggregating systems. For this purpose, growing clusters are substituted by convex nonoverlapping polygonal domains (cells) that form a tessellation of the space where aggregation takes place. The number of sides and area of each cell denote the number of nearest neighbors and area filled by the real cluster together with its surrounding depletion region, respectively. In our study we go further to the nearest-neighbor clusters and investigate the short- and long-range ordering created by the aggregation process and how this structuring is related to the surface packing fraction of particles.

The paper is organized as follows. Section II describes the basic theoretical aspects of aggregation kinetic and topology, while Sec. III focuses on the long-range topological properties. We tackle the results and discuss the most important remarks in Sec. IV. Finally, Sec. V details the conclusions.

II. KINETICS AND TOPOLOGY OF COLLOIDAL AGGREGATION

The kinetics of aggregation processes are usually described in terms of the cluster-size distribution $\{n_i(t)\}$, defined as the number of cluster formed by i individual colloidal particles. The time evolution of the cluster-size distribution is strongly connected to the particle-particle interactions, the spacial dimensionality, and the geometry of the clusters. One of the most studied properties derived from $\{n_i(t)\}$, is the weight-average cluster size S_w:

$$S_w(t) = \sum_{i=1} i^2 n_i(t) \Big/ \sum_{i=1} i n_i(t). \tag{1}$$

Analogously, the number-average cluster size is defined as $S_n(t) = \Sigma_{i=1} i n_i(t) / \Sigma_{i=1} n_i(t)$. For long aggregation times, it has been observed experimentally and by simulations that the weight-average cluster size develops a power-law behavior, $S_w(t) \sim t^z$, where z is the so-called kinetic exponent. Then, if one represents the function $S_w(t)^2 n_i(t)$ versus a normalized cluster size, $i/S_w(t)$, we see that all the curves can be scaled into a single time-independent scaling function $\Psi(i/S_w(t)) = S_w(t)^2 n_i(t) \, \forall \, t \gg 1$ [7,36]. The shape of this master curve depends on the aggregation regime.

One of the most studied aggregation regimes is the diffusion-limited cluster aggregation (DLCA) [37], which can be considered a reference process because of its simplicity. In this regime, colloidal particles freely move by Brownian diffusion (without interparticle interactions) and they become irreversibly stuck after collision. Therefore, the aggregation process is totally determined by the time involved in the diffusion of the clusters before they collide to form a new larger cluster. The clusters formed under this conditions have an open structure, with a fractal dimension of 1.45 for two dimensions [38] and 1.79 for three dimensions [39,40], while the master curve is bell shaped in both cases [7,8], which means that the monomers and small-sized species are rapidly removed during the aggregation process to form larger clusters.

Another limit for aggregation is described by the reaction-limited cluster-cluster aggregation (RLCA) model. In this model aggregation is prevented by using a low sticking probability for two colliding aggregates [3]. Here, the kinetic properties and the cluster population are mainly determined by the cluster-cluster reaction time, which becomes much larger than the diffusion time. In this regime, the master curve shows a different shape: for two-dimensional aggregation the bell-shaped form broadens significantly [41], while for three dimensions the master curve becomes a monotonous decreasing function of the cluster size [8]. That means that reaction-controlled cluster-cluster coagulation leads to more polydisperse cluster-size distributions and, therefore, to more disordered systems.

The kinetic aspects are essential to understand the *affinity* between clusters with different sizes and to give an estimate of the total aggregation rate. However, the cluster-size distribution $n_i(t)$ only gives information about the population of the different species formed during the aggregation process, but not about the structure and distribution of these clusters in space. In order to understand the short- and long-range structure of the whole system of clusters confined in two dimensions, a topological description is needed. By means of the Voronoi construction, each cluster is replaced first by a point representing its center of mass, and then, the space around each point is partitioned into convex, irregular polygons, called *cells*. What we obtain after this mapping is a disordered tessellation or *froth*, where the original clusters are represented by nonoverlapping cells. Figure 1 illustrates a typical snapshot of the colloidal clusters and the froth derived from this method during the coagulation process.

The number of sides of a cell, n, informs about the number of closest neighboring clusters, while the area of the cell, A, is related to the total area filled by the colloidal cluster and its depletion region. The relative distance between two nonneighboring clusters is now represented by the topological distance j, defined as the minimum number of cells that we must go through from a starting cell to a given final cell (see Fig. 2). The topological distance allows us to consider the froth as a collection of concentric shells which are at the same topological distance from a central *seed*. The main advantage of using the topological distance j instead of the metric distance r is the fact that j gives an unambiguous and time-independent measurement of the coordination shell at which a cluster is localized in relation to a central one. For a system of growing clusters, however, the typical metric distance of a certain coordination shell is not a constant quantity, but it increases as the aggregation proceeds. The topo-

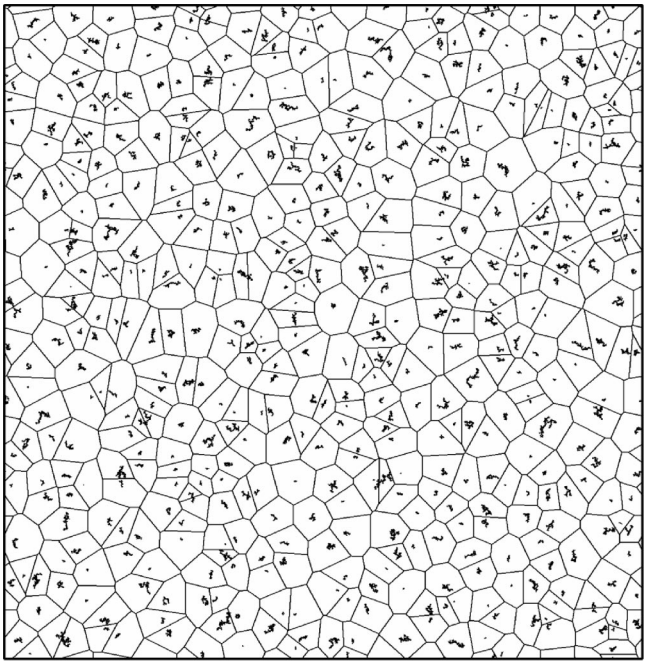

FIG. 1. Typical snapshot of a two-dimensional system of aggregating clusters and the subsequent Voronoi diagram built up from their center of masses.

logical distance also gives a good characterization of the correlation between any couple of cells of the froth (i.e., correlation between two colloidal clusters). Indeed, any modification in the shape or the number of sides of a particular central cell produced by the motion and/or aggregation of the colloidal clusters will have more influence on the cells placed at small topological distances. For large j the statistical properties of the cells become independent of the central one. In fact, as we will see later, the cell-cell correlations are negligible for $j>2$.

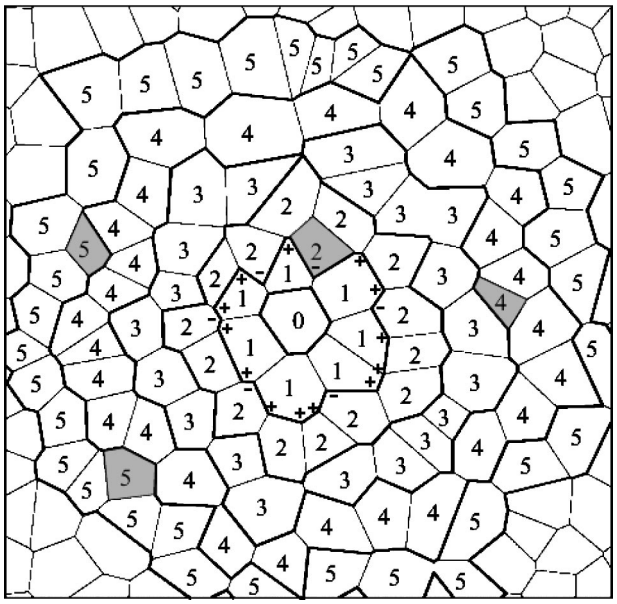

FIG. 2. Cell structure and defects around a given central cell. The number inside the cells is the topological distance from the central cell. The grey cells represent topological defects. The "+" "−" symbol represents the convex (concave) vertexes of the first layer.

In two-dimensional coagulation the evolution of the cellular pattern is ruled by two independent processes. The first one is the diffusive motion of the clusters in the plane: every time a cluster moves a large enough distance, a new rearrangement of the cells is found in terms of a local side switching (also called T1 process). The second process takes place when two clusters coagulate together to form a larger cluster; here, one of the cells disappears and the surrounding cells are accommodated to the new configuration (T2 process) [21]. Both topological processes induce a topological restructuring of the two-dimensional froth that is connected, in general, to the physical conditions of the aggregating system and, more specifically, to the aggregation regime and the packing fraction of particles ϕ_s.

Since the aggregation process induces a disordered froth with irregular cells, the number of sides and area of the cells will be statistical properties distributed according to $P(n,A)$, defined as the probability of finding a cell of n sides and area A. Analogously, we can obtain the probability of finding an n-sided cell as $P(n)=\Sigma_A P(n,A)$. The topology of cellular patterns imposes some constraints on the distribution $P(n)$. Defining the average area of an n-sided cell as $A(n)=\Sigma_A AP(n,A)$, we have that

$$\sum_{n=3} P(n)A(n) = \frac{A_0}{N_c}, \tag{2}$$

where A_0 is the area of the whole froth and N_c is the total number of cells (i.e., colloidal clusters). One of the other important constraints which holds for the case of Voronoi diagrams formed by trivalent cell's vertexes on a Euclidean two-dimensional space is the so-called Euler theorem [42]. It states that the average number of sides of a cell is 6:

$$\langle n\rangle = \sum_{n=3} P(n)n = 6. \tag{3}$$

One of the most interesting quantities derived from the probability distribution $P(n)$ is its second central moment, $\mu_2=\langle n^2\rangle-\langle n\rangle^2=\Sigma_{n=3}(n-6)^2P(n)$, which can be understood as an estimate of the degree of the disorder in the froth.

In principle, n and A are both essential to give a complete description of the froth. However, only one of them is really necessary since these quantities are in fact strongly correlated through the Lewis' law, which states that the mean area of the n-sided cells shows a linear dependence on n, $A(n)=\kappa(t)(n-n_0)$ [43]. Here, $\kappa(t)$ increases with the aggregation time whereas n_0 is found to be a constant value [16]. Hence, the number of sides n is sufficient to give a good representation of the froth and the cluster-cluster correlations.

The study of correlations between the shapes of two neighboring cells in the froth can be easily done with the help of $m_1(n)$, defined as the average number of sides of the adjacent cells of n-sided cells. From space-filling conditions follows the result that large cells (i.e., with many sides) tend to be surrounded by small cells. This intuitive property can be expressed in a semiempirical law called the *Aboav-Weaire*

law [44,45], which states that on average $m_1(n)$ is linear in $1/n$:

$$m_1(n) \approx (6-a) + \frac{6a+\mu_2}{n}, \tag{4}$$

where μ_2 is again the second central moment and a is the screening factor. This law can be exactly deduced from the evolution of an ideal froth where the T2 transformations are restricted to the disappearance of three-sided cells, which gives a screening parameter of $a=1$ [28]. In many natural froths a is of the order of 1 [45]. For two-dimensional coagulation, however, the T2 processes are due to the aggregation between pair of clusters. That allows the removing of cells with more than three sides, so the screening factor can take, in principle, values different to 1 too.

III. LONG-RANGE TOPOLOGICAL CORRELATIONS OF THE VORONOI CONSTRUCTION

As we have seen in the previous section, the analysis of two-dimensional cellular patterns can be performed by means of several laws regarding the evolution of the probability $P(n)$ and the correlations between adjoining cells (Aboav-Weaire law). However, these descriptions are mean-field treatments and do not include the correlations between nonadjoining cells. In order to describe the correlations between any pair of aggregating clusters in the whole system, we need the topological distance. In general, any trivalent froth can be studied by means of a shell structure around a central cell. The first layer (with $j=1$) corresponds to the nearest-neighbor cells, the second layer to the cells adjoining the first layer, etc.

This decomposition of the plane in concentric regions allows us to systematically explore the long-range ordering induced by the coagulation process and to measure the topological distances at which a colloidal cluster "feel" the presence of a second cluster. From a topological point of view, what we are looking for is to describe how the fact of having an n-sided cell affects the whole froth and to give an estimate of the topological distance $j=\xi$ where the correlations vanish. If ξ is large, then the cells in the froth are strongly correlated and mean-field models break down. On the contrary, for $\xi=1$ only the adjoining cells are influenced by the central seed, and for $\xi=0$ we find a totally uncorrelated system (topological gas).

A. Definitions and basic properties

Some j-dependent topological quantities are required in order to describe the structure of concentric shells. Here we will follow the notation introduced in Ref. [32]:

$K_j(n)$: average number of cells in the j layer around an n-sided central cell.

$m_j(n)$: average number of sides of the cells in the j layer around an n-sided central cell.

$q=6-n$: topological charge of an n-sided cell.

$Q_j(n)=\Sigma_{i\leqslant j}[6-m_i(n)]K_i(n)$: total topological charge of the cells that go from the central seed to the j layer.

$C_j(n,m)$: probability of finding an m-sided cell at a distance j from an n-sided cell.

$V_j^+(n)$: average number of convex vertexes going from the j layer to the $(j+1)$ layer around an n-sided central cell (represented as $+$ symbols in Fig. 2).

$V_j^-(n)$: average number of concave vertexes going from the j layer to the $(j-1)$ layer around an n-sided central cell (represented as $-$ symbols in Fig. 2).

As we will see later, most of this quantities are connected among them. In particular, it is specially interesting to write down the relationship between the topological charge and the number of convex and concave vertexes, which reads [32]

$$Q_j(n) = 6 - V_j^+(n) + V_j^-(n). \tag{5}$$

We can define the corresponding n averages of $K_j(n)$, $m_j(n)$, and $Q_j(n)$, which no longer depend on the number of sides of the central cell—i.e., $\langle K_j\rangle=\Sigma_{n=3}K_j(n)P(n)$, $\langle m_j\rangle=\Sigma_{n=3}m_j(n)P(n)$, and $\langle Q_j\rangle=\Sigma_{n=3}Q_j(n)P(n)$. We can introduce the fluctuations of the topological charge as

$$\Gamma_j(n) = Q_j(n) - \langle Q_j\rangle. \tag{6}$$

In the particular case of a froth where the Aboav-Weaire law holds, it can be shown that the fluctuation at the first layer $j=1$ is given by

$$\Gamma_1(n) = (1-a)(6-n). \tag{7}$$

By definition, a froth is completely uncorrelated when the probability $C_j(n,m)$ factorizes as [34]

$$C_j^{un}(n,m) = P(n)P(m)\frac{K_j(n)K_j(m)}{\langle K_j\rangle^2}. \tag{8}$$

Hence, $\beta_j^{n,m}=C_j(n,m)/C_j^{un}(n,m)$ is a measure of the correlations between cells. If $\beta_j^{n,m}$ is lower than 1 for some particular value of j, it means that these kind of cells "repel" each other in a topological sense. On the contrary, for $\beta_j^{n,m}>1$ we find an attraction of affinity between n and m cells at a distance j. In particular, for $j=1$ the Aboav-Weaire law imposes an attraction between dissimilar cells and repulsion between cells with the same number of sides $(n=m)$. At large enough topological distances $(j\gg 1)$ the correlations vanish and so $\beta_{j\to\infty}^{n,m}\to 1$.

In any two-dimensional Euclidean system the number of cells per layer, $K_j(n)$, tends to be a linear function of the topological distance for $j\gg 1$:

$$K_j(n) = Cj + B(n), \quad j \gg 1. \tag{9}$$

Since at such large distance the froth is also uncorrelated $(j>\xi)$, it follows that C must be a constant number independent of the number of sides of the central cell. Analogously, the shape of the central cell is irrelevant at large j, and so the average number of sides of the j-layer cells $[m_j(n)]$ is simply given by the average number of sides of the whole system: i.e.,

$$m_j(n) = \langle n\rangle = 6, \quad j \gg 1. \tag{10}$$

An important statistical property is the so-called generalized sum rule of Weaire, which states that

$$\langle (m_j(n) - n)K_j(n)\rangle = 0. \tag{11}$$

This rule holds for any value of the topological distance j and for any kind of froth. By using this general property and assuming that we are in a j layer where the cells are uncorrelated from the central cell ($j > \xi$), one finally obtains the following expression for the topological fluctuations:

$$\Gamma_j(n) = \Gamma_{j-1} + \langle (6-n)K_j(n)\rangle \left[\frac{K_j(n)}{\langle K_j\rangle} - 1 \right], \quad j > \xi. \tag{12}$$

B. Topological defects

We can distinguish two different types of cells in any j layer of the shell structure. The cells connecting neighbors from the layers $j-1$ and $j+1$ belong to the *skeleton* of the froth. The cells that have neighbors in the $(j-1)$ layer but not in the $j+1$ are called *defects*. Figure 2 illustrates an example of a shell structure with topological defects (gray cells). The total cells of a j layer will be separated into skeleton (K_j^{sk}) and defective K_j^d types—i.e., $K_j(n) = K_j^{sk}(n) + K_j^d(n)$.

Topological defects are in fact folds of the shell structure and, as μ_2, give a rough estimate of the degree of disorder in the froth. Indeed, they are not present in perfectly ordered froths (as hexagonal or rectangular lattices), but only in such systems where the Voronoi diagram is not constituted by regular cells. In our case, the Voronoi construction derived for a time-dependent two-dimensional system of aggregating clusters is definitively a nonordered process, so the quantification of the number of defects during the coagulation will give a characterization of the evolution of the cluster-cluster correlations.

Without defects the outgoing convex vertexes from the j layer are equal to the incoming concave vertexes to the $(j+1)$ layer—i.e., $V_j^+(n) = V_{j+1}^-(n)$. However, if topological defects are present in the froth, part of the outgoing vertexes are trapped in the defective cells. In this case, the previous relation does not hold any more and a correction must be included in order to consider the lost of outgoing vertexes. One obtains

$$V_{j+1}^- = V_j^+ - \eta K_{j+1}^d, \tag{13}$$

where η is the average number of sides lost in one defect. Note that we have explicitly omitted the dependence of η on the number of sides of the central seed (n) and the topological distance j since the value of this quantity is found to be rather constant for all the defects in the whole system and close to 1.

C. Particular case: $\xi = 2$

If we have a system where the adjoining cells verify the Aboav-Weaire law and where the cell-cell correlations vanish after the second layer $\xi = 2$, then it is possible to find simple expressions for the most important topological quantities. Using the exact relation

$$V_j^-(n) = K_j^{sk}(n) = K_j(n) - K_j^d(n), \tag{14}$$

together with Eqs. (5), (6), (11), and (13), and following the demostration given by Aste *et al.* in Ref. [32], we find that the number of cells of the second and third shells [$K_2(n)$ and $K_3(n)$] can be approximated by

$$K_2(n) = 12 + \mu_2 + (2-a)(n-6) + (1-\eta)K_2^d(n),$$

$$K_3(n) = 18 + (4-a)\mu_2 + \left(3 - 2a + \frac{(2-a)^2\mu_2}{12+\mu_2}\right)(n-6) - \eta K_2^d(n) + (1-\eta)K_3^d(n). \tag{15}$$

From these equations, we can obtain an explicit expression for the asymptoic value of the average topological charge, $\langle Q_j\rangle$. Using the definition of the topological charge and the generalized sum rule of Weaire [Eq. (11)], we obtain

$$\langle Q_j\rangle - \langle Q_{j-1}\rangle = \langle [6 - m_j(n)]K_j(n)\rangle = \langle (6-n)K_j(n)\rangle. \tag{16}$$

In the asymptotic limit, $K_j(n)$ is given by Eq. (9). Hence,

$$\langle Q_j\rangle - \langle Q_{j-1}\rangle = \langle (6-n)\rangle Cj + \langle (6-n)B(n)\rangle = \langle (6-n)B(n)\rangle, \quad j \geqslant \xi. \tag{17}$$

As can be seen, the difference $(\langle Q_j\rangle - \langle Q_{j-1}\rangle)$ is independent of the topological distance. In other words, the topological charge inside a layer is constant. Assuming now that $\xi = 2$ and using Eq. (15), we have

$$\langle Q_j\rangle - \langle Q_{j-1}\rangle = \langle (6-n)K_2(n)\rangle = -(2-a)\mu_2, \quad j \geqslant 2, \tag{18}$$

where the contribution of the defects has been neglected. By iterating last expression, it follows that

$$\langle Q_j\rangle = -(2-a)\mu_2(j-1) + \langle Q_1\rangle, \tag{19}$$

where $\langle Q_1\rangle$ is the average topological charge contained up to the first layer. It is given by $\langle Q_1\rangle = \langle 6-n\rangle + \langle [6-m_1(n)]n\rangle = \langle (6-n)n\rangle = -\mu_2$. The final form for $\langle Q_j\rangle$ is then

$$\langle Q_j\rangle = -\mu_2(2-a)j + (1-a)\mu_2. \tag{20}$$

By combining Eqs. (5), (13), and (14), the following expression for the average topological charge in the j layer is found:

$$\langle Q_j\rangle = \langle 6 - V_j^+ + V_j^-\rangle = 6 + \langle -V_{j+1}^- - \eta K_{j+1}^d + V_j^-\rangle = 6 + \langle K_j - K_{j+1} - K_j^d + (1-\eta)K_{j+1}^d\rangle. \tag{21}$$

We can deduce an analytic expression for C, the slope of $K_j(n)$ for large j, by taking the asymptotic limit $j \gg 1$ and using Eqs. (9) and (20) in Eq. (21):

$$-(2-a)\mu_2 j = 6 - C + (1-\eta)K_{j+1}^d - K_j^d. \tag{22}$$

It is appropriate to define the proportion of defects in the j layer as the ratio $\Lambda_j = \langle K_j^d\rangle / \langle K_j\rangle$. With this definition and using Eq. (9), the last equation can be written as

$$-(2-a)\mu_2 j = [(1-\eta)\Lambda_{j+1} - \Lambda_j]Cj + (6-C) + (1-\eta)\Lambda_{j+1}(B+C) - \Lambda_j B. \quad (23)$$

In the asymptotic limit, the proportion of defects converges to a constant value independent of j, $\lim_{j\to\infty}\Lambda_j \equiv \Lambda$. Hence,

$$-(2-a)\mu_2 j = \eta\Lambda Cj + \text{const}, \quad (24)$$

where const is a value independent of j. The matching of both terms for $j \gg 1$ imposes the following identity for the slope C:

$$C = \frac{(2-a)\mu_2}{\eta\Lambda}, \quad (25)$$

which predicts that C is directly correlated to the short- and long-range disorder of the froth (μ_2 and Λ, respectively). Finally, if $\langle K_j \rangle$ shows a linear dependence already for $j > 2$, then the average number of sides lost in defects η can be approximated by [32]

$$\eta = \frac{\mu_2(2-a)}{[6+(3-a)\mu_2]\Lambda}. \quad (26)$$

In the next section, the short- and long-range topological properties derived from $P(n;t)$ and the correlations between neighboring and non-neighboring cells of the shell structure will be studied for two-dimensional aggregation processes. Since colloidal coagulation is a time-dependent process, both the probability and cell-to-cell correlations will be a function of the aggregation time. Therefore, $P(n;t)$ will be the probability of finding an n-sided cell at time t, $K_j(n;t)$ will be the average number of cells in the j layer around an n-sided cell at time t, and so on.

IV. RESULTS AND DISCUSSION

The purpose of this work is to study how the aggregation process affects the topological properties of a system of colloidal clusters. The topological correlations will be then a direct consequence of the spatial structuring of the space-filling system of clusters. We have neglected the particle-particle interactions in order to pick up solely the effects of the pure diffusive aggregation (DLCA) and the monomer concentration on the behavior of the topological properties. Brownian dynamics off-lattice DLCA simulations were performed, in a square box of side L by considering a total number of monomers of $N_0 = 30\,000$ with a particle diameter $d = 735$ nm and for five different packing fractions: $\phi_s = N_0\pi r^2/L^2 = 0.005$, 0.01, 0.03, 0.06, and 0.1. In the initial state, monomers were placed at random avoiding particle-particle overlapping. Periodic boundary conditions are imposed at the boundaries of the simulation surface. The simulations were stopped when the number of clusters was around 1500 aggregates. For the entire surface packing fractions considered this condition is enough to reach the scaling time and it is a warranty to have good statistics for all aggregation times.

The diffusion coefficient (D) of a single cluster is obtained from its radius of gyration (R_g) assuming Stokes' law $D \sim 1/R_g$. To move the aggregates they are selected one by one for a movement test. A random number ξ uniformly distributed in [0;1] is generated. If $\xi \leqslant D/D_{max} = (R_g)_{min}/R_g$, the cluster is moved in a random direction. If $\xi > D/D_{max}$, the cluster does not move. D_{max} is the largest diffusion coefficient and $(R_g)_{min}$ the smallest radius gyration in the whole system of clusters. Whether the cluster moves or not, the time is increased by

$$\Delta t = \frac{1}{ND_{max}}. \quad (27)$$

A collision is considered to occur when a moved aggregate overlaps another one. Then, the position of the moved cluster is corrected backwards along the direction of the movement as far as the surfaces of both clusters are in contact. These contacting clusters are joined to form a larger cluster that will continue the diffusive motion in the following time step. For DLCA every collision produces coagulation. More technical details of the simulations can be found in Ref. [16].

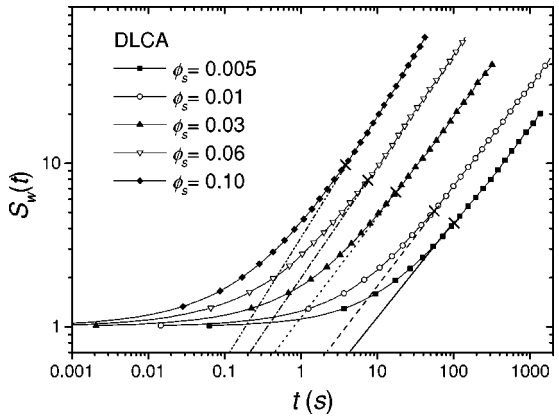

FIG. 3. Time evolution of the weight-average cluster size obtained from DLCA simulations for five surface packing fractions. At long times, $S_w(t)$ shows a power-law behavior (scaling). The cross symbols represent the scaling time t_{sc}.

A. Topological ordering between nearest neighbor clusters in the scaling regime

In Fig. 3, the weight-average cluster size is plotted as a function of the aggregation time for the five surface packing fractions. $S_w(t)$ monotonically increases as time goes on, and after the so called scaling time t_{sc} (see cross symbols), it reaches the scaling behavior given by a power-law growth: $S_w(t) \sim t^z$. For higher particle concentrations the aggregation process is faster, and consequently the scaling region is manifested at shorter times with a larger kinetic exponent z [46] (see Table I).

After this brief description of the kinetic properties, we will focus on the topological aspects of the aggregation process. For all the studied situations (i.e., different times and initial particle concentration conditions), the probability of number of sides $P(n)$ was a centered distribution around the maximum value at $n = 6$ and the first moment verified the

TABLE I. Kinetic exponent z and scaling time t_{sc} for the five surface packing fractions studied in this work.

ϕ_s	z (±0.01)	$t_{sc}(s)$
0.005	0.60	101.7
0.01	0.61	55.8
0.03	0.63	17.1
0.06	0.68	7.4
0.10	0.76	3.8

Euler theorem ($\langle n\rangle=6$). The second central moment μ_2 determines the dispersion of $P(n)$, so it can be regarded as the key quantity to characterize the global topological disorder of the system of clusters. As shown in Fig. 4, μ_2 decreases with time for all cases for short times. However, after a certain time which corresponds to the scaling time t_{sc} it finally reaches a roughly time-independent value. This long-time behavior has been previously observed by several authors [15,17,19]. Indeed, experiments on soap froths indicate that, as time goes on, there is a final state where the topological properties reach stable values [32]. Some experiments of two-dimensional colloidal coagulation performed by Earnshaw and Robinson also show similar topological results for $t>t_{sc}$ [15].

The decrease of μ_2 reveals that the clusters formed in the DLCA regimen tend to adopt a hexagonal-like structure as the aggregation proceeds; i.e., the aggregation process induces a topological ordering that is intimately related to the spatial organization of the clusters in the plane. As soon as the scaling of the cluster-size distribution is manifested, the topological ordering ends and the system of aggregating clusters reaches a final stationary state with constant μ_2. Therefore, the dynamic scaling can be understood as a "stationary" state in a topological point of view. Our simulation results also show that the final stationary value of μ_2 decreases as the particle concentration increases (from $\mu_2=1.42$ for $\phi_s=0.005$ to $\mu_2=1.07$ for $\phi_s=0.1$), which means

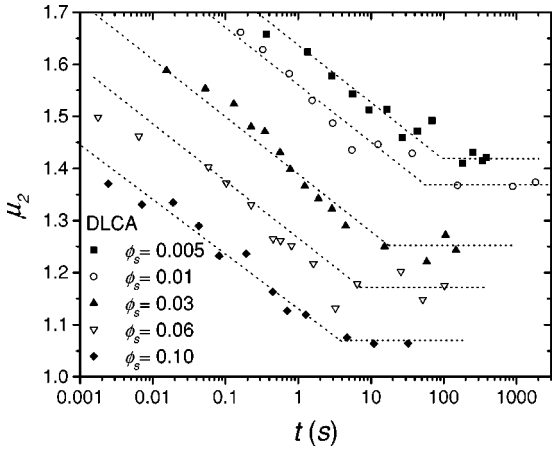

FIG. 4. Second central moment of $P(n)$ as a function of the aggregation time for five surface packing fractions. After the scaling time μ_2 reaches a final stationary value (dashed lines are only guides for the eyes).

that aggregation induces stronger topological ordering for dense colloidal suspensions than for the dilute ones.

In terms of the intercluster structure, this ordering is linked to the growth of the colloidal clusters and the existence of free space between them. Clusters are noncompact fractal-type structures with a special ability to fill the space even for a relatively small number of particles. The typical distance between the surfaces of two nearest-neighbor clusters $[r_s(t)]$ is given by

$$r_s(t) = r_{cc}(t) - 2R(t), \tag{28}$$

where $r_{cc}(t)$ is the average distance between centers of the clusters and $R(t)$ is the characteristic cluster radius. r_s is a measure of the size of the depletion zone around a cluster. The cluster growth is achieved at the expense of the surrounding particles and clusters, which are mopped up after diffusion through this depletion distance. When the dynamic scaling is established, the fractal dimension of the clusters d_f is a well-defined quantity and $R(t)$ scales with the number-average cluster size as $R(t)\sim S_n(t)^{1/d_f}$. The center-to-center distance is, however, given by $r_{cc}(t)\sim S_n(t)^{1/2}$. Since $d_f<2$, we observe that $R(t)$ grows faster than $r_{cc}(t)$. At very low particle concentrations, this effect is not really important since the average cluster-cluster distance is much larger than the cluster radius at any aggregation time. However, for higher particle densities, the free space available between a cluster and its nearest neighbors becomes rapidly small compared to the effective surface filled by the fractal clusters. Then, the cluster structure is able to induce spatial order in the cluster localization: the surrounding clusters around a central one tend to adopt a more closely packed two-dimensional structure (the more particle density we have, the stronger is the intercluster ordering). Topologically, it yields the increase of six-sided cell probability and the subsequent reduction of μ_2 for more dense systems and long aggregation times. Since this effect is a consequence of the trend of fractal clusters to fill up the whole space, we do not expect the same spatial organization when clusters are not fractal. This is the case of aggregation into a finite energy minimum, which allows the colloidal particles to rearrange inside the cluster and to form more compact structures [47].

The final stationary value for μ_2 obtained during the scaling regime seems to be an intrinsic property of the self-assembly of the clusters linked to the value of the average fractal dimension of the cluster. In fact, we expect departures from our results for μ_2 at very high particle densities and long times, when the aggregating system is close to undergo gelation ($r_s\approx 0$), since the clusters lose their individual fractal character and become homogeneous structures (with $d_f=2$).

A similar steady-state behavior is found for screening factor a obtained using the Aboav-Weaire law and the average number of sides of the nearest-neighbor cells of an n-sided cell, $m_1(n)$. The inset in Fig. 5 shows $m_1(n)$ as a function of $1/n$ for the particular case of $\phi_s=0.01$ after the scaling time (similar curves are found for the rest of particle concentrations and aggregation times). This means that large clusters (with many number of sides) tend to be surrounded by small

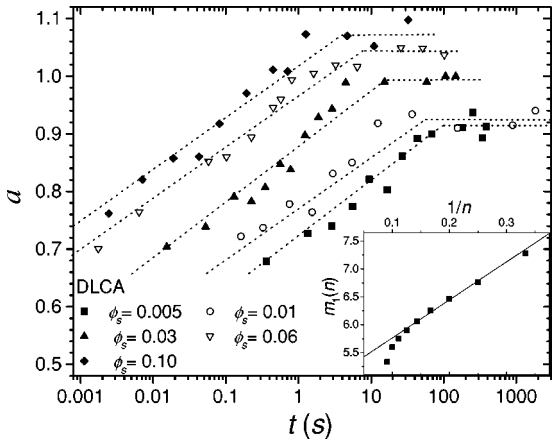

FIG. 5. Screening factor a calculated by fitting $m_1(n)$ according to the Aboav-Weaire law [cf. Eq. (4)]. After the scaling time a also reaches a stationary value (dashed lines are only guides for the eyes). Inset: average number of sides of the cells adjacent to an n-sided cell calculated for $\phi_s=0.01$ after the scaling time ($t=893$ s). The straight solid line represents the fit using the Aboav-Weaire law.

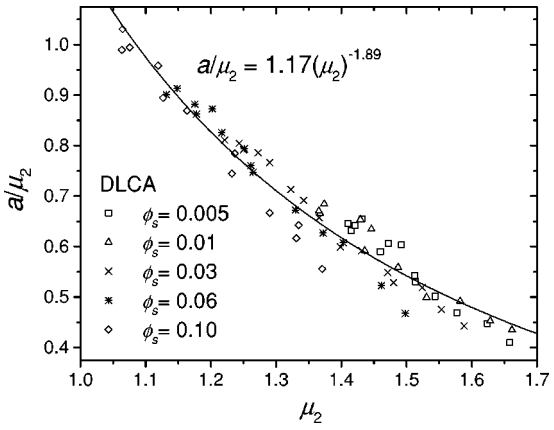

FIG. 6. The simulated μ_2 and a/μ_2 data at any time and for the five studied particle concentrations lie in a universal common form: $a/\mu_2=1.17(\mu_2)^{-1.89}$. In this plot, the μ_2 axis is representative of the time axis, but in the opposite direction.

ones (with low n). Together with the simulated data, we represent the fit using the Aboav-Weaire law given by Eq. (4) (solid line). As observed, simulated and theoretical $m_1(n)$ agree well, except for the cells with large number of sides ($n>9$) where departures from the Aboav-Weaire prediction are found due to statistical uncertainties.

The screening factor a obtained from the fits of $m_1(n)$ is not an independent property but it is also strongly correlated to the topological order of the system. In fact, for most of the froths with weak and moderate disorders, a is a positive quantity and grows as μ_2 decreases [48]. This behavior is also found for the particular case of two-dimensional colloidal coagulation. Indeed, as observed from Fig. 5, the parameter a first increases for times below the scaling time and arrives at a rather stationary state when the dynamic scaling is established. The final value of a increases with particle density, going from $a=0.91$ for $\phi_s=0.005$ to $a=1.07$ for $\phi_s=0.1$. Moreover, if we represent the simulated values of a/μ_2 for all times and for the five different surface packing fractions of particles as a function μ_2, the results lie in a universal curve (see Fig. 6), given by $a=D(\mu_2)^w=1.17(\mu_2)^{-0.89}$. A similar universal behavior is found for other natural or computer-simulated froth systems but with different values of D and w [35,48]. Since the exponent w may be considered as a universality class feature of the froth evolution, we deduce that the topological structuring induced by two-dimensional aggregation processes corresponds to a unique universality class ($w=-0.89$) which no longer depends on the monomer density, but it is a general property linked to the space-filling aspects of the cluster growth.

B. Correlations between nonadjacent clusters

This section extends the study of the topological properties beyond the first nearest-neighbor cells. First we investigate the average number of cells around an n-sided cell for the two nearest nonadjacent layers with respect to the central seed: $K_2(n)$ and $K_3(n)$. Figure 7 shows an example of the dependence of the simulated $K_2(n)$ and $K_3(n)$ on the number of sides (symbols) together with the theoretical prediction (lines) deduced for froths where the cell-cell topological correlations vanish after the second layer [see Eq. (15)] and where the first cell is correlated according to the Aboav-Weaire law. As observed, this theoretical model reproduces fairly well the simulation data, although some departures are found for cells with $n\geqslant 9$ as a consequence of the failure of the Aboav-Weaire law for such many-sided cells (see the inset of Fig. 5.) Although the complete set of results is not shown, similar agreement between theory and simulation was found for all aggregation times and particle densities, supporting the idea that the aggregation process is incapable of producing correlations for $j>2$. Moreover, the values of $K_2(n)$ and $K_3(n)$, which characterize the shape of the second and third layers of the shell structure, are basically given by

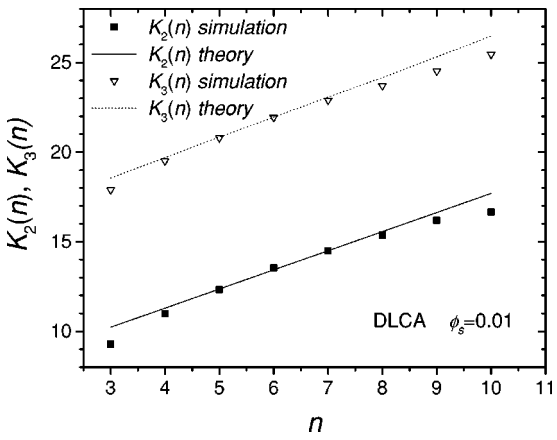

FIG. 7. Dependence of the average number of cells in the closest nonadjacent layers to the central one, $K_2(n)$ and $K_3(n)$, on the sides number n for DLCA simulations with $\phi_s=0.01$ after the scaling time. The solid lines represent the theoretical expectations obtained using Eqs. (15). Similar fittings are obtained for all simulations.

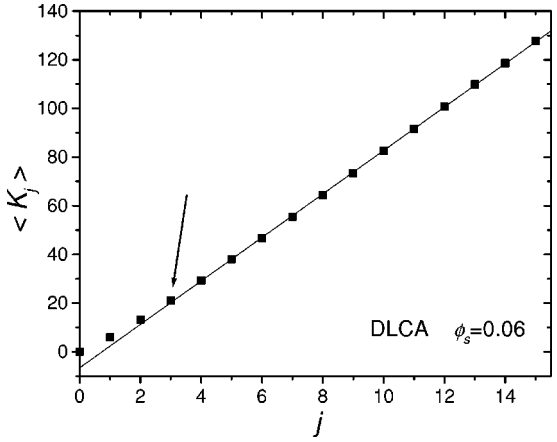

FIG. 8. Dependence of the average number of cells $\langle K_j \rangle$ on the topological distance j for DLCA simulation with $\phi_s = 0.06$ after the scaling time. $\langle K_j \rangle$ grows linearly for $j > 2$.

topological properties related to single-cell averages and first-layer correlations, as the second central moment μ_2 and a.

In the next step we go beyond the first three nearest layers with the aim of studying the long-range topological properties and their asymptotic limit. Using the quantities defined in Sec. III, we can describe the long-range ordering of the froth induced by the aggregation process. First of all, we start our analysis with the average number of cells $\langle K_j \rangle$ and the average topological charge $\langle Q_j \rangle$. Figures 8 and 9 show a typical example of the dependence of both quantities on the topological distance for the particular case of $\phi_s = 0.06$. On the one hand, $\langle K_j \rangle$ shows a linear growth with the topological distance after the second layer ($j > 2$). On the other hand, the topological charge decreases also linearly with j. Moreover, $\langle Q_j \rangle$ is well described by the theoretical prediction $\langle Q_j \rangle = -\mu_2(2-a)j$ given in Eq. (20) for froths where the cell-cell correlations vanish after the second layer. Similar results are found for all times and other particle densities.

Both results corroborate an already mentioned fact: the spatial and topological correlations between two clusters are

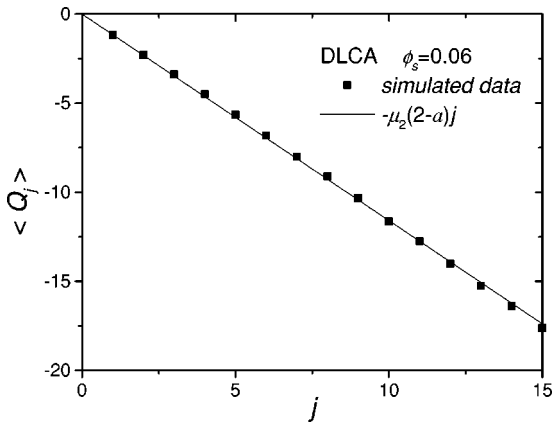

FIG. 9. Dependence of the average topological charge $\langle Q_j \rangle$ on the topological distance j for DLCA simulations with $\phi_s = 0.06$ after the scaling time (square symbols). The straight line is the theoretical prediction $\langle Q_j \rangle = -\mu_2(a-2)j$.

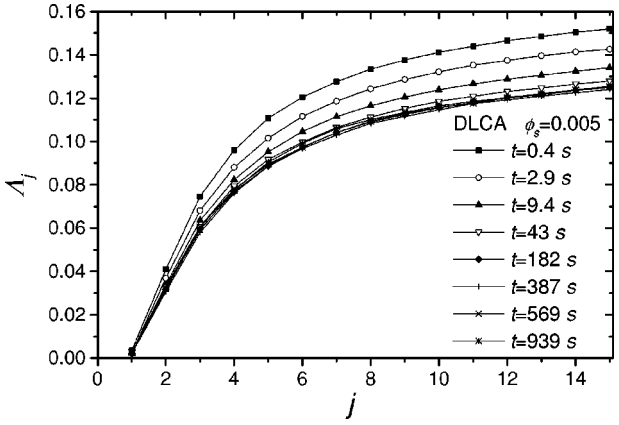

FIG. 10. Proportion of defects as a function of the topological distance obtained for a DLCA simulation with $\phi_s = 0.005$. In the scaling regime ($t > t_{sc} \approx 100$ s), the curves become time independent.

negligible if the topological distance between them is larger than 2. This conclusion has been independently confirmed by measuring the probabilities $C_j(n,m)$ for several values of n and m (not shown). Indeed, the amplitude of the oscillations of $\beta_j^{n,m} = C_j(n,m)/C_j^{un}(n,m)$ is only important for $j = 1,2$ and becomes insignificant for $j > 2$. Furthermore, since Eq. (20) holds for all particle concentrations and aggregation times (before and after the scaling), we conclude that the aggregation process is only able to induce short-range intercluster correlations (up to $j = \xi = 2$) even at high particle packing fraction: clusters in the third layer do not feel the properties of a given central one.

We now turn to the study of another important aspect of the froth: the topological defects. Their presence in the shell structure has a dramatic influence on the cell assembly. In fact, for froths with large values of the proportion of defects, Λ_j, the cell-cell correlations drop off very fast with the topological distance j. It means that cluster-cluster correlations beyond nearest neighbors are mainly dominated by the percentage of defects.

Figure 10 shows the proportion of defects as a function of j for several aggregation times for the particular case of $\phi_s = 0.005$ (similar curves are found for the other particle densities). In all cases Λ_j increases with j, and for large distances it reaches an asymptotic constant value Λ, which features the long-range shell structure. As the coagulation progresses, the whole curves go down and reach lower values of Λ. This decrease of the defect concentration as time evolves clearly indicates that the aggregation process induces ordering not only between nearest neighbors ($j = 1$), but also between well-removed clusters ($j \gg 1$). It is remarkable that, for times beyond the scaling time ($t_{sc} \approx 100$ s), the curves saturate and the topological ordering of the froth arrives at a stationary state.

This behavior can be better observed if we represent the asymptotic value of the proportion of defects Λ as a function of time (see Fig. 11). Unfortunately, our simulated data go up to topological distances $j \leqslant 15$ and we do not have valuable information at larger distances. This is mainly because of the poor statistics that we have for such large distances, espe-

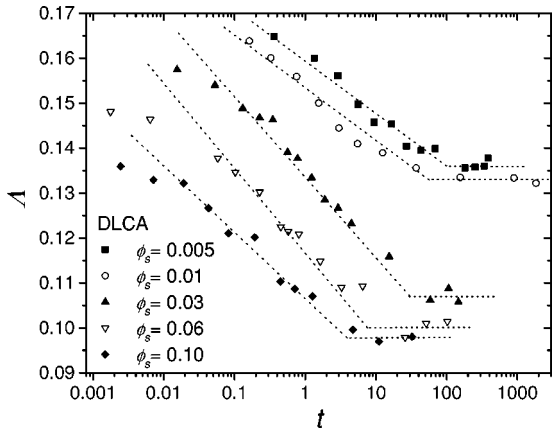

FIG. 11. Asymptotic value of the proportion of defects as a function of the aggregation time for the five studied surface packing fractions. After the scaling time Λ reaches a final stationary value (dashed lines are only guides for the eyes).

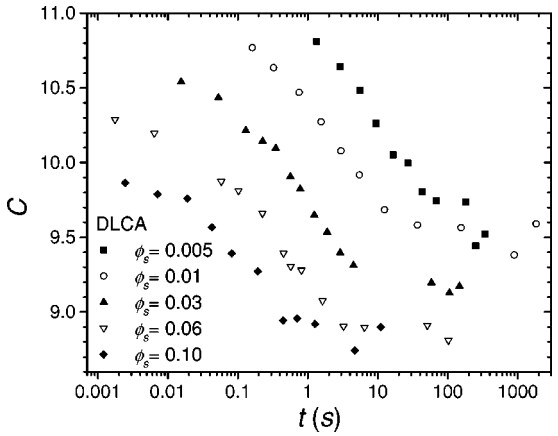

FIG. 12. Time evolution of the slope C of $\langle K_j \rangle$ for the five studied surface packing fractions. After the scaling time C also has a constant value.

cially for long aggregation times, where the number of clusters is small and the analysis becomes affected by the boundaries of the simulation box. Nevertheless, although the defect concentration shown in Fig. 10 does not reach completely this asymptotic value, there is a clear trend that points out the existence of a constant value for large enough topological distances. This constant value is rather logical since there is no difference between any shell and the next one for large values j. We refer the reader to Ref. [32], where a similar behavior for the proportion of defects is observed and a final asymptotic stabilization is found. In this respect, our asymptotic value is in fact an extrapolation of the simulated data for large j.

In order to estimate this parameter, the simulated data have been fitted according to the following empirical law:

$$\Lambda_j = \Lambda + \frac{\Lambda_1 - \Lambda}{1 + \left(\frac{j-1}{j_0}\right)^p}, \tag{29}$$

where Λ is the asymptotic value for $j \gg 1$, Λ_1 is the percentage of defects for the first layer, and p and j_0 are fitting parameters. The regression coefficient was $r > 0.99$ in all fittings and the value for the parameter p was 1.6 ± 0.1 for all times and surface packing fractions.

What we obtain is a plot which resembles the one obtained for μ_2 (cf. Fig. 4); i.e., Λ decreases with the aggregation time for $t < t_{sc}$ and becomes constant for $t > t_{sc}$. Once more the arrangement provoked by the aggregation is more important for higher particle concentrations: the average value found in the scaling regime decreases as we increase the surface packing fraction up to $\phi_s = 0.1$. As discussed in Sec. IV A for μ_2 and a parameters, the decrease of the number of defects at all topological distances also accounts for the fact that fractal cluster growth at high particle concentrations leads to stronger density modulation of the system and so to more structured close-packed structures (an ideal hexagonal froth has $\mu_2 = 0$, $a = 0$ and $\Lambda = 0$).

By using the simulated values of Λ, μ_2, and a into expression (26) we can calculate theoretically the average number of sides lost in the defective cells, η. The behavior of η does not show clear tendencies with aggregation time or particle density. On the contrary, it remains roughly constant for all the studied situations and is given by $\eta = 1.2 \pm 0.1$.

Finally, we study the behavior of the slope C, obtained from the fitting of $\langle K_j \rangle$ in the asymptotic limit. The results are shown in Fig. 12 for the five studied particle densities and times before and after the scaling. Again we observe different behavior between the early stages of the aggregation (where C decreases monotonically with t) and the final stationary value found in the scaling regime. Particularly, C takes values close to 11 at the beginning of the coagulation and decays to a final value that is smaller at higher particle concentrations (from $C = 9.57$ for $\phi_s = 0.005$ to $C = 8.82$ for $\phi_s = 0.1$).

The quantity Cj can be understood as the average perimeter of a j layer. For perfect spherical layers the value of C should be $2\pi \approx 6.28$. However, the C values calculated from the DLCA computer simulations are always higher at all aggregation times and particle densities, which is evidence for the roughness of the shell structure, due not only to the fact that the cells do not form a smooth circle, but also to the presence of topological defects. Indeed, shell structures with many defective cells will have layers of larger perimeter and higher values of C. This fact establishes a connection between C and the defect concentration Λ (C decrease with Λ). Therefore, the long-range topological order induced by the aggregation process is also the responsable of the decrease in C with t during the prescaling regime.

The comparison between the simulated results for C and the theoretical prediction given in Eq. (25) for froths uncorrelated after the second layer is generally in good agreement. Although some departures are observed between simulated data and theory, they are mainly due to statistical errors in the determination in the parameters involved in such expression. It proves that C is not an independent variable, but it is attached to the values of μ_2, a, and Λ. Similar dependences have been observed throughout this work for several topological quantities, as $K_2(n)$, $K_3(n)$, and $\langle Q_j \rangle$. Since the

asymptotic value of the defect concentration Λ is also linked to the global disorder in the froth (set by μ_2), we conclude that all the short- and long-range topological properties in the system of aggregating clusters are controlled by the screening factor a and the second central moment μ_2. Both parameters are mean-field properties that characterize the global disorder and the correlation between nearest-neighbor clusters, but do not inform anything about the long-range structure. Thus, we find the surprising fact that the long-range order is determined by average properties involving only single-cell and nearest-neighbor correlations.

In our opinion, the fact that the long-range correlations are determined by average properties as the second central moment μ_2 and the parameter a is basically a consequence of the lack of cell-cell correlations for topological distances beyond the second concentric layer, $j>2$. It allows us to express the topological properties for $j>2$ as functions of the properties for $j\leqslant 2$, which are mainly given by μ_2 and a. One good example of this may be seen in the study of the average topological charge $\langle Q_j\rangle$ [see Eqs. (18), (19), and (20)], where the lack of cell-cell correlations for $j>2$ leads to an expression for $\langle Q_j\rangle$ only in terms of the properties of cells with $j\leqslant 2$, as $K_2(n)$ and $\langle Q_1\rangle$, which, in turn, are given in terms of μ_2 and a. For such froths where the topological correlations reach larger distances, this simple scheme will not hold any more and a more sophisticated description will be called for.

It should be note that these results obtained for two-dimensional (2D) cluster-cluster aggregation cannot be, in principle, extrapolated to other types of space-filling structures. For instance, the correlations between cells can be important even for $j>2$, and then all the theoretical expressions shown above will break down.

V. CONCLUSIONS

We studied the time evolution and topological properties of computer-simulated two-dimensional aggregating systems for several surface packing fractions of particles. We assumed the simplest case of freely Brownian diffusive sticking particles without interactions (DLCA). The topological properties have been measured with the help of the Voronoi construction, which replaces the original system of aggregating clusters by an equivalent system of convex nonoverlapping regions (cells) that completely tessellate the plane, each cell representing a single cluster of the system and its surrounding depletion zones. The study of the correlations between nonadjacent cells was achieved by analyzing the system as structured in concentric layers around a given central one. This method allows us to go beyond the internal fractal structure of the clusters and to study the external intercluster properties. Indeed, it determines the short- and long-range spatial organization and the cluster-cluster "interactions" induced by the mutual competition between neighboring depletion regions that occurs when the fractal-like clusters fill up the whole space.

We found that the topological aspects of the aggregation are strongly connected to the kinetic ones. In all cases, we obtained a continuous ordering of the cell structure as aggregation proceeds. Specifically, clusters tend to adopt a more ordered hexagonal organization in the plane, which topologically means a reduction in both the second central moment of the number of sides distribution μ_2 and the proportion of defects Λ. This ordering is more important for higher particle densities, where the already small free space existing between growing clusters becomes rapidly shrunk due to the fractal growth. This ordering finishes as soon as the scaling of the cluster-size distribution is reached ($t>t_{sc}$). Since all the studied topological properties [$P(n)$, μ_2, a, $\langle K_j\rangle$, $\langle Q_j\rangle$, and Λ] remain constant in this final scaling limit, it can be regarded as a topological-invariant state. We also found that the whole coagulation process (after and before the dynamic scaling) lies in a universal topological class independent of the particle concentration, given by the general relation $a\sim\mu_2^{-0.89}$.

After the comparison of the simulated data and the theoretical expressions, we concluded that colloidal aggregation in two dimensions is only able to produce short-range intercluster correlations (up to the second layer of clusters around a central one, $j=2$) even for the very high packing fraction of particles. However, the ordering is manifested in the whole shell structure at any topological distance in terms of a decrease of the proportion of defective cells Λ_j. Finally, we obtained that the main topological property that controls the degree of structuring at short and long intercluster distances is the second central moment μ_2, which is a measurement of the global order in the whole system.

Future investigations will involve the study of the area distribution of the cells $P(A)$ [defined as $P(A)=\Sigma_{n=3}^{\infty}P(n,A)$] of a system of clusters under coagulation in two dimensions. Particularly, it would be interesting to know the time evolution and scaling properties in the long-time scaling state. Moreover, since each cell corresponds to a colloidal cluster formed by a certain number of particles i, one could construct the distribution $P(n,A,i)$, as the probability of finding an n-sided cell with area A that contains a clusters of size i. The correlation between these three variables will give us a direct relation between kinetic features (that comes through i) and the topological ones (n and A). Finally, in a logical step forward, it is highly interesting to extend the topological and structural description to three-dimensional aggregating systems of dense colloidal suspensions and to colloidal systems with interacting particles as those with long-range particle-particle repulsive interactions. Note the difference between our results and earlier results in 3D [13,14], where it is found that, after the depletion region, the particle-particle correlation function tends to 1 after reaching the nearest-neighbor clusters, without further oscillations in this function (besides those coming for the statistical uncertainties). It is possible that the clusters in 3D, due their ability to interpenetrate more easily without touching [46], "feel a lower repulsion between them," while in 2D the greater "repulsion" would make the clusters to become more ordered, increasing in this way the ξ to a value equal 2. Or perhaps the absence of further oscillations is due to having considered the particle-particle correlations function and not the cell-cell correlations as in the present work. All this merit a similar study for the three-dimensional case, as stated above.

ACKNOWLEDGMENTS

The authors acknowledge the financial support from Spanish "Ministerio de Educación y Ciencia, Plan Nacional de Investigación (I+D+i), MAT 2003-08356-C04-01," by the "European Regional Development Fund," (ERDF) and the DGAPA/UNAM (Proyecto PAPIIT IN118705-2).

[1] Z. Hórölgyi, G. Medveczky, and Z. Zrínyi, Colloids Surf. **60**, 79 (1991).
[2] D. J. Robinson and J. C. Earnshaw, Phys. Rev. A **46**, 2045 (1992).
[3] D. J. Robinson and J. C. Earnshaw, Phys. Rev. A **46**, 2055 (1992).
[4] F. Guezzi and J. C. Earnshaw, J. Phys.: Condens. Matter **9**, L517 (1997).
[5] J. C. Fernández-Toledano, A. Moncho-Jordá, F. Martínez-López, and R. Hidalgo-Álvarez, Langmuir **20**, 6977 (2004).
[6] A. Moncho-Jordá, F. Martínez-López, A. E. González, and R. Hidalgo-Álvarez, Langmuir **18**, 9183 (2002).
[7] P. Meakin, T. Vicsek, and F. Family, Phys. Rev. B **31**, 564 (1985).
[8] M. L. Broide and R. J. Cohen, Phys. Rev. Lett. **64**, 2026 (1990).
[9] M. Carpineti and M. Giglio, Phys. Rev. Lett. **68**, 3327 (1992).
[10] D. J. Robinson and J. C. Earnshaw, Phys. Rev. Lett. **71**, 715 (1993).
[11] M. Carpineti, M. Giglio, and V. Degiorgio, Phys. Rev. E **51**, 590 (1995).
[12] M. D. Haw, M. Sievwright, W. C. K. Poon, and P. N. Pusey, Physica A **217**, 231 (1995).
[13] A. E. González and G. Ramírez-Santiago, Phys. Rev. Lett. **74**, 1238 (1995).
[14] A. E. González and G. Ramírez-Santiago, J. Colloid Interface Sci. **182**, 254 (1996).
[15] J. C. Earnshaw and D. J. Robinson, Physica A **214**, 23 (1995).
[16] A. Moncho-Jordá, F. Martínez-López, and R. Hidalgo-Álvarez, Physica A **282**, 50 (2000).
[17] J. C. Earnshaw and D. J. Robinson, Phys. Rev. Lett. **72**, 3682 (1994).
[18] M. Marder, Phys. Rev. A **36**, 438 (1987).
[19] J. Stavans and J. A. Glazier, Phys. Rev. Lett. **62**, 1318 (1989).
[20] J. Stavans, Phys. Rev. A **42**, 5049 (1990).
[21] J. J. Chae and M. Tabor, Phys. Rev. E **55**, 598 (1997).
[22] B. Dubertret, K. Y. Szeto, and W. Y. Tam, Europhys. Lett. **45**, 143 (1999).
[23] A. Abd el Kader and J. C. Earnshaw, Phys. Rev. E **58**, 760 (1998).
[24] W. Y. Tam, Phys. Rev. E **58**, 8032 (1998).
[25] P. S. Sahni, D. J. Srolovitz, G. S. Grest, M. P. Anderson, and S. A. Safran, Phys. Rev. B **28**, 2705 (1983).
[26] J. C. M. Mombach, R. M. C. de Almeida, and J. R. Iglesias, Phys. Rev. E **48**, 598 (1993).
[27] W. Korneta, S. K. Mendiratta, and J. Menteiro, Phys. Rev. E **57**, 3142 (1998).
[28] N. Rivier, Philos. Mag. B **52**, 795 (1985).
[29] J. R. Iglesias and M. C. de Almeida, Phys. Rev. A **43**, 2763 (1991).
[30] K. Y. Szeto and W. Y. Tam, Phys. Rev. E **53**, 4213 (1996).
[31] T. Aste, D. Boosé, and N. Rivier, Phys. Rev. E **53**, 6181 (1996).
[32] T. Aste, K. Y. Szeto, and W. Y. Tam, Phys. Rev. E **54**, 5482 (1996).
[33] T. Aste, Phys. Rev. E **55**, 6233 (1997).
[34] K. Y. Szeto, T. Aste, and W. Y. Tam, Phys. Rev. E **58**, 2656 (1998).
[35] K. Y. Szeto, X. Fu, and W. Y. Tam, Phys. Rev. Lett. **88**, 138302-1 (2002).
[36] G. Odriozola, A. Moncho Jordá, A. Schmitt, J. Callejas Fernández, R. Martínez García, and R. Hidalgo Álvarez, Europhys. Lett. **53**, 797 (2001).
[37] E. J. W. Verwey and J. Th. C. Overbeek, *Theory of the Stability of Lyophobic Colloids* (Elsevier, Amsterdam, 1948).
[38] M. Kolb, R. Botet, and R. Jullien, Phys. Rev. Lett. **51**, 1123 (1983).
[39] R. Jullien and R. Botet, *Aggregation and Fractal Aggregation* (Word Scientific, Singapore, 1987).
[40] T. Vicsek, *Fractal Growth Fenomena*, 2nd ed. (World Scientific, Singapore, 1992).
[41] D. J. Robinson and J. C. Earnshaw, Phys. Rev. A **46**, 2065 (1992).
[42] N. Rivier and A. Lissowski, J. Phys. A **15**, L143 (1982).
[43] F. T. Lewis, Anat. Rec. **38**, 341 (1928).
[44] G. Le Caër and R. Delannay, J. Phys. A **26**, 3931 (1993).
[45] D. A. Aboav, Metallography **13**, 43 (1980).
[46] A. E. González, F. Martínez-López, A. Moncho-Jordá, and R. Hidalgo-Álvarez, Physica A **314**, 235 (2002).
[47] W. Y. Shih, J. Liu, W. H. Shih, and I. A. Aksay, J. Stat. Phys. **62**, 961 (1991).
[48] R. Delannay and G. Le Caër, Phys. Rev. Lett. **73**, 1553 (1994).